Shabnam Raayai-Ardakani[1]
Department of Mechanical Engineering,
Massachusetts Institute of Technology,
Cambridge, MA 02139
e-mail: shraayai@mit.edu

Jose Luis Yagüe
IQS—Grup d'Enginyeria de Materials,
Universidad Ramon Llull,
Barcelona 08017, Spain
e-mail: jose.yague@iqs.url.edu

Karen K. Gleason
Department of Chemical Engineering,
Massachusetts Institute of Technology,
Cambridge, MA 02139
e-mail: kkg@mit.edu

Mary C. Boyce
School of Engineering and Applied Science,
Columbia University,
New York, NY 10027
e-mail: boyce@columbia.edu

Mechanics of Graded Wrinkling

The properties and behavior of a surface as well as its interaction with surrounding media depend on the inherent material constituency and the surface topography. Structured surface topography can be achieved via surface wrinkling. Through the buckling of a thin film of stiff material bonded to a substrate of a softer material, wrinkled patterns can be created by inducing compressive stress states in the thin film. Using this same principle, we show the ability to create wrinkled topologies consisting of a highly structured gradient in amplitude and wavelength, and one which can be actively tuned. The mechanics of graded wrinkling are revealed through analytical modeling and finite element analysis, and further demonstrated with experiments. [DOI: 10.1115/1.4034829]

1 Introduction

The surface of many plants and animals possesses textural features which are either periodic or random in nature with spacings and amplitudes of length scales from nanometers to hundreds of microns or even larger. Such textures provide plants and animals with enhanced interaction with the surrounding environment, including tailored attributes such as wettability, antifouling, adhesion, and hydrodynamics. For example, the scales of a large number of shark species are covered with tiny ribs aligned in the streamwise direction. This ribbed structure of a shark scale has been shown to reduce the wall shear stress by up to 10% while also exhibiting self-cleaning abilities [1–3]. The height and spacing of the riblets are seen to vary between 100–500 μm and 100–300 μm, respectively, with each scale possessing one to seven riblets [2]. Also, surfaces of rice leaves and butterfly wings are covered by hierarchical structures and directed grooves along the length of the leaves, allowing the leaves to control the flow direction of droplets [4–6].

In this work, we use the idea of wrinkling to create ribbed structures to achieve a graded texture inspired by the shark skin. Wrinkling of the thin film occurs when the film is in compression and reaches a buckling condition [7–9]. Wrinkled surfaces have been fabricated with a variety of methods such as prestretching the soft substrate, depositing a thin film, and releasing the stretch [10–12]; ultraviolet ozone (UVO) treatment of stretched elastomers followed by release of the stretch [13]; focused ion beam treatment of the stretched elastomers [14]; solvent swelling and shrinkage of a laterally confined elastomer [15–17]; and constrained thermal expansion/shrinkage [18]. Fabrication conditions can induce initially uniform uniaxial and biaxial loading or stress states that, respectively, yield uniaxial wave forms [9,11,17,18] or various biaxial wave forms [10,19,20]. The presence of inclusions in a composite system or other induced material or stress-state nonuniformities can produce a stress gradient stemming from the irregularity which gives a gradient in the wrinkle profile [21]. Here, we reveal the mechanics of graded wrinkling through analytical modeling and finite element simulations, showing the ability to create highly structured wrinkled topologies with prescribed gradients in amplitude and wavelength; this phenomenon is then demonstrated with representative example cases of a stiff polymer coating deposited on a soft substrate using initiated-chemical vapor deposition (iCVD).

2 Background: Uniform Uniaxial Wrinkling

Wrinkling is a terminology used to refer to the buckling of a thin stiff film that is bonded to a relatively softer substrate where a compressive stress state is imposed to the film by different methods. If the bilayer is compressed only in one direction, it results in a uniaxial wrinkling waveform of repeating wavelength and amplitude. This periodic wrinkling phenomenon can be explained through energy minimization: during compression of the film, buckling will become energetically favorable over uniform compression; when bonded to a substrate, the film buckling will act to locally stretch the substrate, and hence the favorable energy state will be a wavelength that finds the minimum total energy of the buckled film and locally stretched substrate. Thus, through scaling of the strain energy in the film and the substrate and assuming a sinusoidal wrinkle profile, the critical wavelength at which wrinkling occurs is found to be proportional to the thickness of the film (t) as well as the ratio of the modulus of the film (E_f) and the substrate (E_s) to the one-third power ($\lambda \sim t(E_f/E_s)^{1/3}$) [22].

For the case of a uniform axial compression in the film (here referred to as uniform wrinkling), the profile of the thin wrinkled film is a sinusoidal wave ($A\sin(\lambda x)$) with the same wavelength (λ) and amplitude (A) everywhere (Fig. 1). Wrinkling can be modeled as an eigenvalue problem using beam theory for the thin film and an Airy stress function analysis for the substrate, taking both materials to be linear elastic. The effect of the buckled film on the substrate and vice versa is modeled as a distributed load at the substrate surface to determine the surface traction [7]. This

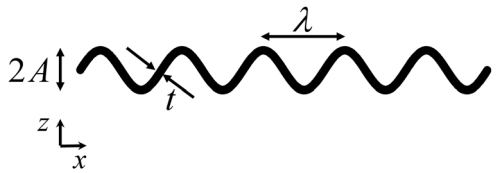

Fig. 1 Schematic of uniform wrinkling

[1]Corresponding author.

Manuscript received September 11, 2016; final manuscript received September 22, 2016; published online October 13, 2016. Editor: Yonggang Huang.

simplified model results in a fourth-order ordinary differential equation (ODE) for the wrinkle profile, and, by assuming a sinusoidal profile, the ODE can be solved for the critical strain (Eq. (1)) and critical wavelength (Eq. (2)) at which wrinkling initiates. The analytical solution of the resulting governing equation in uniform wrinkling confirms the scaling laws found earlier [7–9,11].

$$\varepsilon_{\text{cr}} = \frac{1}{4}\left(\frac{3E_s}{E_f}\right)^{\frac{2}{3}} \tag{1}$$

$$\lambda_{\text{cr}} = 2\pi t\left(\frac{E_f}{3E_s}\right)^{\frac{1}{3}} \tag{2}$$

Using a simple kinematic model also referred to as the "accordion model," the amplitude of the waves after initiation of the wrinkles can be found. This model assumes the contour length of the film to be constant [11].

$$A_0 = t\sqrt{\frac{\varepsilon}{\varepsilon_{\text{cr}}} - 1} \tag{3}$$

Equation (3) is valid for small imposed strains, and under finite deformation, the amplitude and the wavelength can be approximately found from Eqs. (4) and (5) [10,11].

$$\lambda \approx \frac{\lambda_{\text{cr}}}{1+\varepsilon} \tag{4}$$

$$A \approx \frac{A_0}{\sqrt{1+\varepsilon}} \tag{5}$$

3 Graded Uniaxial Wrinkling

A stress gradient can be induced by either a geometric gradient, an inclusion, or other inhomogeneity. A gradient causes the wrinkles to change from a uniform waveform to a graded wrinkle where the amplitude and/or the wavelength of the wrinkles are not constant along the length of the film. Here, the case of a stress gradient induced by an axial geometry gradient is analyzed. Figure 2 depicts a schematic of a linearly tapered geometry with taper angle θ and a uniform geometry subjected to an axial load, both having constant film thickness. The ratio of $\eta = L/b_L$ is the size of the rectangle bounding either the uniform or tapered geometries. In case of the trapezoid, the combination of $\tan\theta$ and L/b_L would be sufficient to define the geometry completely. The axial force in the film, P_f, is constant as a function of axial position x, but the axial stress varies.

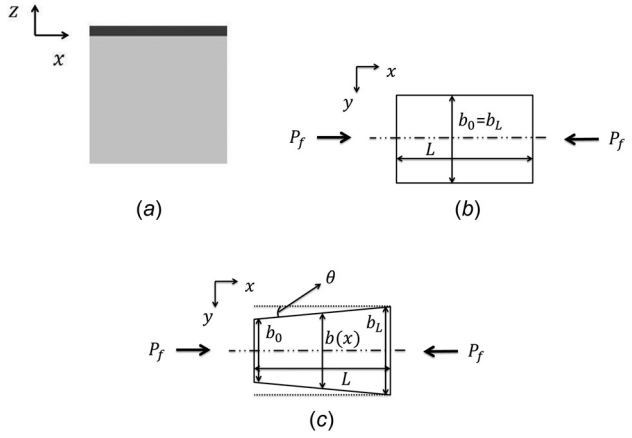

Fig. 2 Free body diagram of the film with $\eta = L/b_L$ in uniform and graded wrinkling subject to compressive force P_f: (*a*) side view of either uniform or graded geometry, (*b*) top view—uniform geometry, and (*c*) top view—graded geometry with taper angle θ

$$P_f(x) = P_f$$

$$\sigma_f(x) = \frac{P_f}{tb_L\left(1 - 2\frac{L}{b_L}\tan\theta + 2\frac{x}{b_L}\tan\theta\right)} = \frac{P_f}{tb_L\left(1 - 2\tan\theta\,\eta\,\frac{L-x}{L}\right)} \tag{6}$$

Similar to the analytical modeling for the case of uniform wrinkling [7,8], analysis of the graded wrinkling is performed using the eigenvalue problem that results from the equilibrium equations for the thin film and the soft substrate. The thin film is modeled as a linear elastic plate of E_f, bonded to a half space of another linear elastic material ($E_s < E_f$). The effect of the film on the substrate is represented as a distributed traction (σ_{zz}) on the plate surface, and vice versa. The general form of the governing equation for wrinkling of the film can be presented as in the following equation:

$$\frac{\partial^2}{\partial x^2}\left(E_f I_f \frac{\partial^2 w}{\partial x^2}\right) + P_f \frac{\partial^2 w}{\partial x^2} + \sigma_{zz} b(x) = 0 \tag{7}$$

where P_f is the compressive load on the film, w is the displacement of the film in the z direction, E_f is the Young's modulus of the film, and $b(x)$ is the width of the film. Based on the form of solution found in uniform wrinkling, it can be assumed that the distributed load in the graded case has a form of

$$\sigma_{zz} b(x) = C\frac{\partial^2 w(x)}{\partial x^2} \tag{8}$$

where C is found using the equilibrium equations for the substrate (without knowing the exact function for w). Therefore, in the case of the tapered geometry, the eigenvalue equation can be rewritten as

$$\frac{\partial^2}{\partial x^2}\left(\frac{b(x)}{b_L}\frac{\partial^2 w}{\partial x^2}\right) + \Lambda^2 \frac{\partial^2 w}{\partial x^2} = 0 \tag{9}$$

with

$$\Lambda^2 = \frac{P_f + C}{\frac{b_L t^3}{12}E_f} \tag{10}$$

where Λ is the eigenvalue, and b_L (Fig. 2(*c*)) is the largest width of the film which is at $x = L$. (Detailed solution to the eigenvalue problem in Eq. (9) is presented in the Appendix.) Thus, the critical eigenvalue corresponding to the onset of buckling is found to be (Eq. (11))

$$\Lambda_{\text{cr}} = \frac{1}{t}\left(\frac{3E_s}{E_f}\right)^{\frac{1}{3}}\sqrt{K} \tag{11}$$

$$K = \frac{L}{b_L}\frac{2\tan(\theta)}{\ln\left(\frac{b_L}{b_0}\right)} = \frac{-2\tan\theta\,\eta}{\ln(1 - 2\tan\theta\,\eta)} = \frac{1 - \frac{b_L}{b_0}}{\ln\left(\frac{b_0}{b_L}\right)} \tag{12}$$

where $\eta = L/b_L$. At the limit of $K \to 1$ or $\eta \tan\theta \to 0$ (i.e., the trapezoid is a rectangle), Eq. (11) will reduce to the critical

eigenvalue found in the analysis for uniform wrinkling $\Lambda_{cr,uniform} = 1/t(3E_s/E_f)^{1/3}$ which is inversely proportional to the critical wavelength reported in Eq. (2). The nondimensional geometric expression K (in Eq. (12)), which shows up in Eq. (11), can be used to compare different graded geometries.

We note that K depends on b_0/b_L and also note that $b_0/b_L = 1 - 2\tan\theta\,\eta$. We will focus on the effect of the two nondimensional geometric parameters $\tan(\theta)$ and η separately and together in the form of K on graded wrinkling. The solution to the eigenvalue problem can be found to be of the form of a Bessel function of the first kind (J_1) as shown in Eq. (13), where the geometric parameter, K, is included through presence of the eigenvalue, Λ_{cr}, in the equation

$$\begin{aligned} w(x) &= C_1 \int\int \frac{J_1\left(\frac{\Lambda_{cr}L}{\tan\theta\,\eta}\sqrt{1-2\tan\theta\,\eta\frac{x}{L}}\right)}{\sqrt{1-2\tan\theta\,\eta\frac{x}{L}}}\,dx\,dx + C_2x^2 \\ &\quad + C_3x + C_4 \\ &= \frac{-C_1}{\Lambda_{cr}^2}\sqrt{1-2\tan\theta\,\eta\frac{x}{L}}\;J_1\left(\frac{\Lambda_{cr}L}{\tan\theta\,\eta}\sqrt{1-2\tan\theta\,\eta\frac{x}{L}}\right) \\ &\quad + C_2x^2 + C_3x + C_4 \end{aligned} \tag{13}$$

The first term in Eq. (13) can be used to find the critical wavelength in graded wrinkling numerically; the results of the calculations are presented in Sec. 6.2.

For comparison, stress and strain profiles in the film prior to wrinkling are presented together with eigenvalues. Taking the case of a thin film bonded to a substrate where the cross-sectional area of the film and the substrate ($b_0 \times t = b_L \times t$) is uniform as shown in Fig. 2(*b*) and subject to compression results in a uniform stress and strain distribution over the length of the film. Thus, the film will wrinkle in a uniform sinusoidal wave upon reaching a critical stress, and the wrinkles will have the same amplitude and wavelength [7,8]. However, a cross-sectional geometry with a gradient will produce a nonconstant stress (Eq. (6)) and strain distribution over the length of the film, and thus wrinkles will not be uniform. Under the same imposed displacement (δ), prior to wrinkling, the strain distribution in a uniform (Eq. (14)) and trapezoidal geometry (Eq. (15)) is found to be

$$\varepsilon_{xx} = \frac{\sigma_{xx}}{E_f} = \frac{\delta}{L} \tag{14}$$

and

$$\begin{aligned} \varepsilon_{xx} &= \frac{\sigma_{xx}}{E_f} = \frac{2\tan(\theta)}{\ln\left(\frac{b_L}{b_0}\right)}\frac{\delta}{b(x)} \\ &= \frac{-2\tan\theta\,\eta}{\ln(1-2\tan\theta\,\eta)}\frac{1}{1-2\tan\theta\,\eta\left(1-\frac{x}{L}\right)}\left(\frac{\delta}{L}\right) \end{aligned} \tag{15}$$

respectively. Since the macroscopic strain in both cases is $\varepsilon_{macro} = \delta/L$, then in uniform wrinkling the ratio of the strain to the macroscopic strain would be one, while in graded wrinkling it will have a form as in the following equation:

$$\frac{\varepsilon_{xx}}{\varepsilon_{macro}} = \frac{K}{\left(1-2\tan\theta\,\eta\left(1-\frac{x}{L}\right)\right)} \tag{16}$$

The ratio of the strain distributions to the macroscopic strains is presented in Fig. 3(*a*) for the uniform geometry ($K = 1$) and graded geometry for the cases with $K = 0.82$ and $K = 0.91$. A plot of the decrease of the normalized eigenvalue ($\Lambda_{cr}/\Lambda_{cr,uniform}$) versus $\eta\tan(\theta)$ and versus $\tan\theta$ for various values of η are shown in Figs. 3(*b*) and 3(*c*) together with $(\Lambda_{cr}/\Lambda_{cr,uniform})^{-1}$ (Fig. 3(*d*)), which can be considered as a normalized characteristic length.

4 Finite Element Analysis

Graded wrinkling was also studied extensively through finite element modeling (FEM). For this purpose, the finite element software ABAQUS was used. In the models, the thickness of the stiff film and the ratio of Young's modulus of the materials were kept constant, and only the geometry of the model (specifically the K parameter) was varied by changing the taper angle (θ—Fig. 2(*c*)) while keeping $\eta = L/b_L$ constant and equal of 5/3. The length of the thin film was chosen to be $L = 200t$, and E_f/E_s is set to 100. The model was compressed to a macroscopic strain of 4% (to avoid going into the nonlinear regime) where the critical strain for the uniform case is 2.4%.

In this study, stress and strain profiles were extracted at different cross-sectional lines ($z = 0$, $z = t/4$, $z = t/2$) along the length (x direction) of the film, as shown in Fig. 4. At strains higher than the critical strain, the stress and strain distributions in the thin film are dominated by bending, and therefore, the stress and strain profiles along different lines will be different. This difference is used in defining the wavelength in graded wrinkling.

5 Experimental Method

Wrinkled surfaces were fabricated following the methods provided in Ref. [10]. Polydimethylsiloxane substrates ($E_{PDMS} \approx 450$ kPa) of thickness of approximately 2 mm were prepared and cut into symmetric trapezoidal geometries (shown in Fig. 5). The substrates were then prestretched to 20% and placed in a vacuum reactor for coating, using initiated-chemical vapor deposition (iCVD). The substrates were coated with iCVD poly(-ethylene glycol diacrylate) (pEGDA, $E_{pEGDA} \approx 775$ MPa and $t \approx 400$ nm) as detailed previously in Ref. [10], and after that, the prestretch was released, putting the film under compression and thus wrinkles were formed. Trapezoidal samples were prepared with different taper angles (θ) and constant $\eta = 25/12$ and thus different values of the K parameter.

The profiles of the wrinkled surfaces were obtained using a Zeta-20 optical profilometer, which gives a three-dimensional image of the surface pattern as well as measuring different dimensions that can be captured in the image [10]. As a result, it is possible to get images of the top view of the wrinkled pattern as well as a three-dimensional view of the same surface [10]. In order to examine the wavelengths and the amplitudes, in each sample, three representative areas were chosen, and the wavelengths and the amplitudes of the waves were measured in those areas. These areas, which represent regions with "largest width (region 1)," "medium width (region 2)," and "smallest width (region 3)," are chosen in arbitrary positions in the corresponding areas (see Fig. 5).

6 Results

6.1 Critical Strain: Analytical Versus FEM. The conditions to initiate wrinkling in the graded case are first examined. The local critical macroscopic strain (at the smallest width of the film (i.e., $b(x = 0) = b_0$)) required to initiate wrinkles is found to increase with an increase in the taper angle (i.e., a greater gradient requires a greater strain to initiate wrinkling). Using the critical eigenvalue in Eq. (11) and substituting back into the definition of the eigenvalue presented in Eq. (9), the critical load at which the buckling occurs can be found. Here, the critical load has been nondimensionalized with the Young's modulus of the film as well as the smallest cross-sectional area (where stress is the highest),

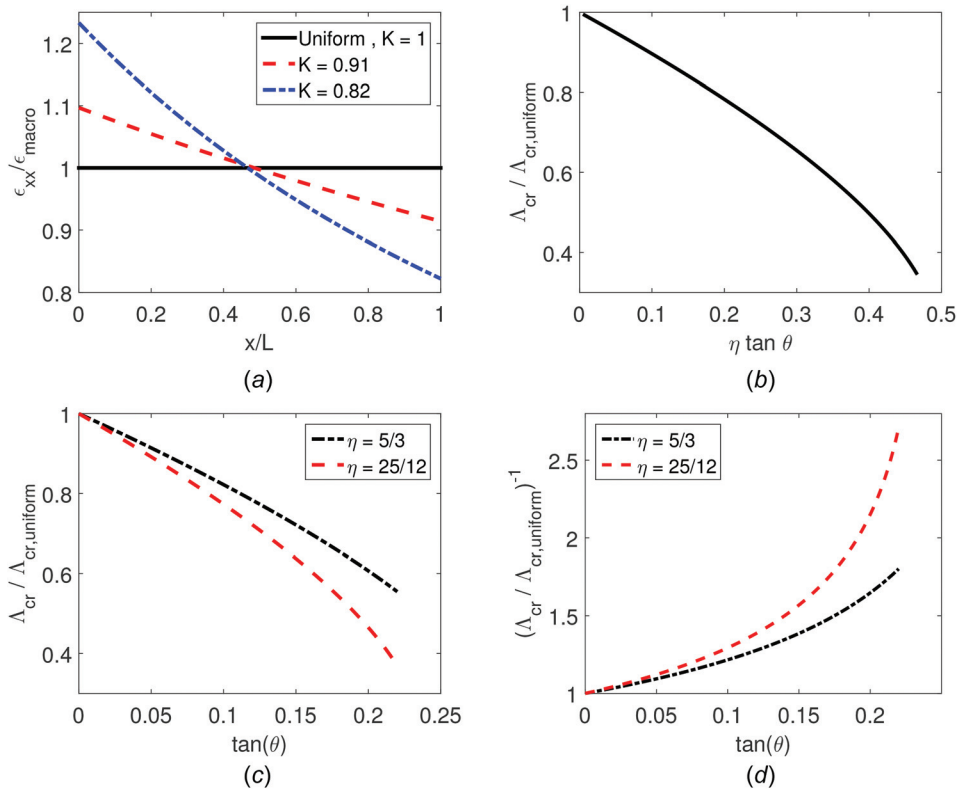

Fig. 3 Strain distribution along the length of the film in graded wrinkling and distribution of the critical eigenvalue in graded wrinkling versus the taper angle and η: (*a*) strain distribution normalized with the macroscopic strain (δ/L) in uniform wrinkling and graded wrinkling corresponding to the geometries with $K = 1$, $K = 0.91$, and $K = 0.81$; (*b*) plot of the critical eigenvalue (Λ_{cr}) in graded wrinkling normalized by the critical eigenvalue in uniform wrinkling ($\Lambda_{cr,uniform}$) versus $\eta \tan(\theta)$; (*c*) plot of the critical eigenvalue (Λ_{cr}) in graded wrinkling normalized by the critical eigenvalue in uniform wrinkling ($\Lambda_{cr,uniform}$) versus $\tan(\theta)$ or different values of η; and (*d*) plot of the inverse of critical eigenvalue (Λ_{cr}) in graded wrinkling normalized by the critical eigenvalue in uniform wrinkling ($\Lambda_{cr,uniform}$) versus $\tan(\theta)$ for different values of η

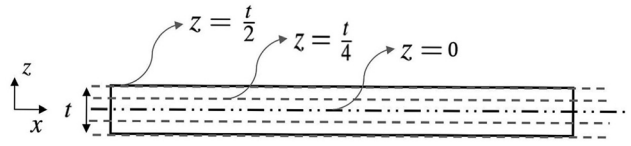

Fig. 4 Longitudinal cross section of the film; the centerline of the film is referenced as $z = 0$, and distances are measured from the centerline. Note that film is in compression and buckling, and hence the neutral axis is not central.

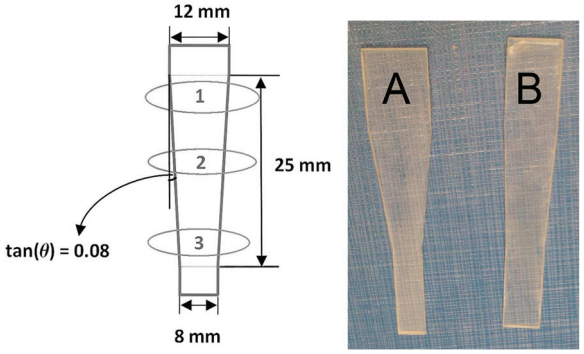

Fig. 5 Schematic of sample geometry with $K = 0.82$ on the left and images of the actual samples on the right where (*A*) corresponds to $K = 0.72$ and (*B*) corresponds to $K = 0.91$

which gives the local critical strain at the smallest width of the film ($x = 0$).

$$\varepsilon_{cr}(x=0) = \frac{P_{cr}}{E_f b_0 t} = \frac{1}{4}\left(\frac{3E_s}{E_f}\right)^{\frac{2}{3}} \frac{K}{1 - 2\tan\theta\,\eta} \tag{17}$$

$$\frac{\varepsilon_{cr}(x=0)}{\varepsilon_{cr,uniform}} = \frac{K}{1 - 2\tan\theta\,\eta} \tag{18}$$

Again at the limit of $K \to 1$ or $(\eta \tan\theta) \to 0$, Eq. (17) will reduce into the expression found for the critical strain in uniform wrinkling.

The results from the finite element post-buckling analysis were used to confirm the analytical solution in Eq. (17). In order to do so, strain data (ε_{xx}) from the region of the smallest width of the film ($b(x=0) = b_0$) were used. Figure 6 shows excellent agreement between the analytical model and the finite element results showing the predictive ability of the analysis, and that with an increase in the taper angle, an increase in the local macroscopic strain at the smallest width of the film, b_0, is needed to initiate wrinkling. Note that since the number of the data points used is limited, an average of the values of the data points close to the transition (from compression to buckling) in the finite element results is used. The error bars show the difference between the average values and the values of the data points in the transition region.

6.2 Critical Wavelength and Wrinkle Evolution: FEM. In uniform wrinkling, wrinkles initiate over the entire length when

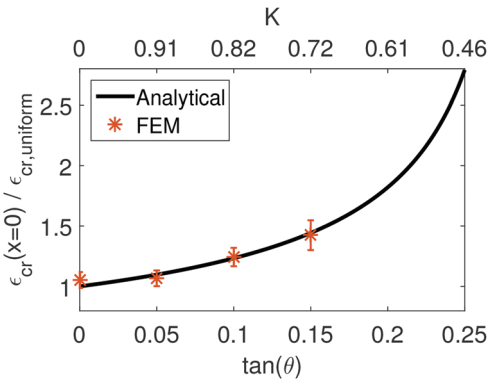

Fig. 6 Critical strain normalized by the critical strain for uniform wrinkling versus K and $\tan\theta$ where $\eta = 5/3$ in graded wrinkling

the critical strain is reached, and the amplitude of each wrinkle increases in the same manner as the macroscopic compressive strain increases. However, a graded geometry creates a nonconstant stress distribution over the length of the film, and thus the wrinkles will not initiate or evolve uniformly over the length.

The evolution plots for uniform wrinkling and for graded wrinkling of a trapezoidal geometry with $K = 0.82$ (result of the finite element analysis) are shown in Fig. 7. The main observations regarding wrinkle evolution are: first, graded wrinkling is a sequential process, meaning that waves initiate along the length in a progressive manner with increasing macroscopic strain. Second, the first wave initiates at the point where the stress is the highest (i.e., the shortest edge (smallest width) of the trapezoid) as expected. Lastly, as the new waves appear with increasing macroscopic strain, the amplitude of the earlier waves increase, and their wavelengths decrease in a manner as expected from the accordion model.

During the sequential formation of graded wrinkling, as different locations along the length reach the critical stress, they start to undergo wrinkling and waves initiate at their critical wavelengths. The critical wavelength of each of the waves can be found using the strain profiles at different macroscopic strains. Figure 8 shows that the critical wavelength of each of the sequentially initiated waves is the same. In addition, as the compressive strain on the film increases, the waves that initiated earlier keep increasing in amplitude, and at the same time their wavelengths decrease. As shown in Fig. 8, λ/t of the third wave decreases by 0.9% as the compressive 2.9% to 3.7% for the case of $K = 0.82$.

The profile of graded wrinkle cases with $K = 0.91$ and $K = 0.82$ as well as the corresponding uniform wrinkles are shown in Fig. 9. Noting from Eq. (16) that the compressive strain varies with position (x) in the graded geometry, in turn, the Poisson effect on the out-of-plane expansion of the substrate $|\varepsilon_{yy}| = \nu_f |\varepsilon_{xx}|$ leads to a gradient in the out-of-plane translation of the film (here, direction z) which are shown with dashed lines on the figures.

The critical wavelength as defined for uniform wrinkling is the wavelength at which wrinkling initiates. Using the strain profiles at different time frames shows that the critical wavelength of each of the consequent waves is the same as the critical wavelength of the initial wave. In Fig. 8, the strain profiles of a wrinkled film at different macroscopic strains are shown, where the critical wavelengths of the waves that are just initiating are specified. As it is seen, the critical wavelength stays constant as the film goes through the sequential wrinkling process, showing that the critical wavelength is independent of position (i.e., x).

Another aspect of critical wavelength in graded wrinkling is the fact that it is dependent on the geometry gradient (K). As it is seen in Fig. 10, the critical wavelengths of trapezoidal films with different taper angles show a modest increase as the taper angle

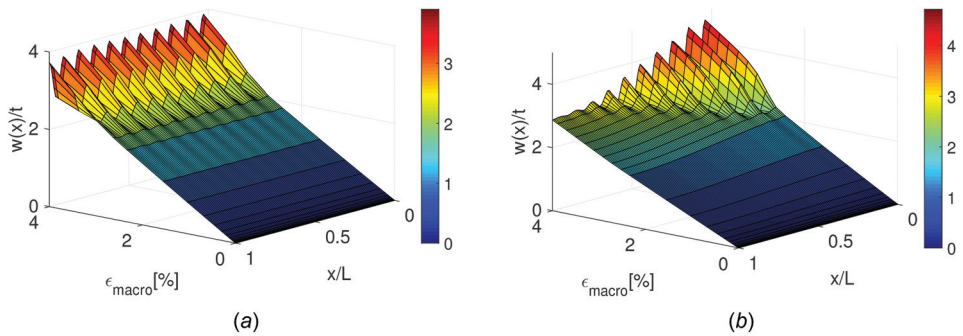

Fig. 7 Wrinkle evolution in uniform and graded wrinkling for the case of $\varepsilon_{macro} = 4\%$: (*a*) uniform wrinkling—$K = 1$ and (*b*) graded wrinkling—$K = 0.82$

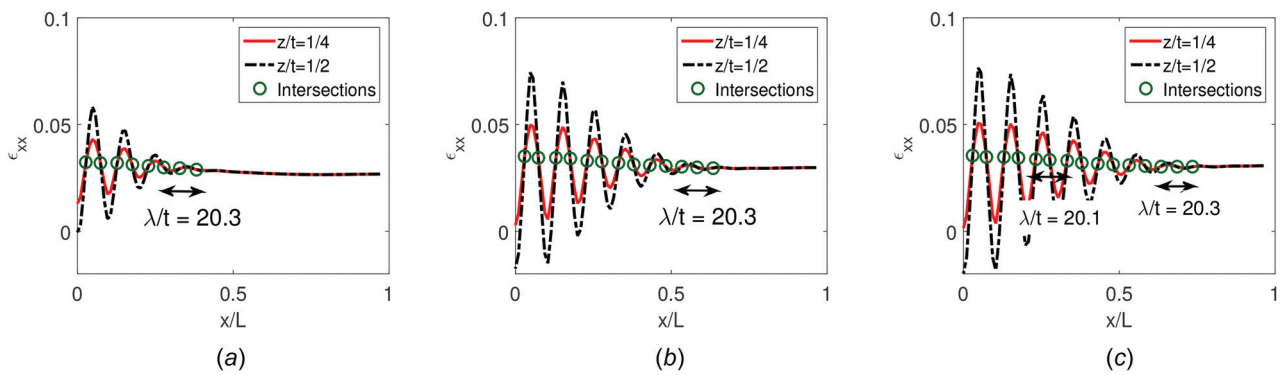

Fig. 8 Strain profiles in graded wrinkling of a trapezoidal geometry with $K = 0.82$ and $E_f/E_s = 100$ at three different compressive macroscopic strains. As the third, sixth, and seventh waves are initiating, they all have $\lambda/t = 20.3$. Also, λ/t of the third wave decreases by 0.9% as the compressive strain is increased by 0.8%. (*a*) $\varepsilon_{macro} = 2.9\%$, (*b*) $\varepsilon_{macro} = 3.5\%$, and (*c*) $\varepsilon_{macro} = 3.7\%$.

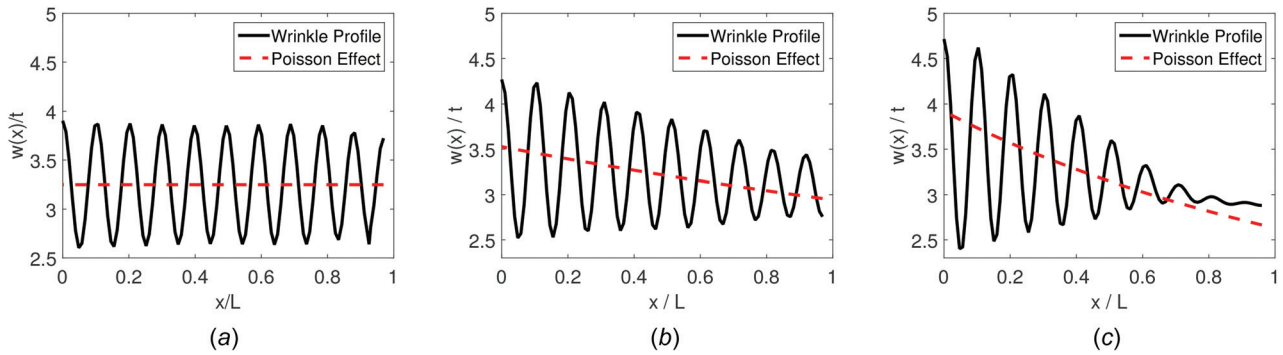

Fig. 9 Wrinkle profile in uniform and graded wrinkling for the case of $\varepsilon_{macro} = 4\%$: (*a*) $K = 1$, (*b*) $K = 0.91$, and (*c*) $K = 0.82$

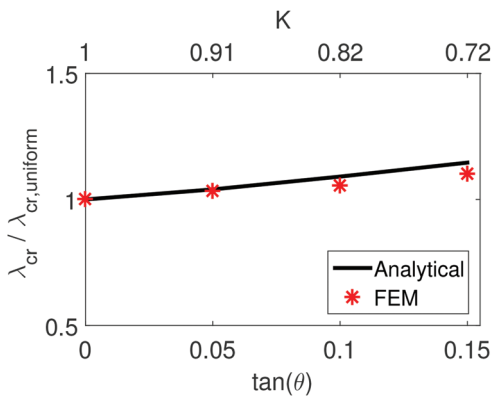

Fig. 10 Critical wrinkling wavelength for different graded geometries with $\eta = 5/3$

increases (η constant) or the K parameter decreases. In other words, the increase in the taper angle gives an increase in the stress gradient within the film, which, in turn, gives an increase in the critical wavelength. Additionally, Eq. (13) can be used to numerically calculate the critical wavelength using the theory. The results of the theory are also shown in Fig. 10.

To further illustrate the graded phenomenon, the finite element result of the strain profiles of two wrinkled surfaces after undergoing 4% of macroscopic strain is presented in Fig. 11. While a uniform geometry under compression results in a sinusoidal strain distribution (Fig. 11(*a*)), the tapered geometries change the strain profile of the wrinkles into waves with higher amplitude at the smaller width (where the stress in the film is the highest) and lowest amplitude at the largest width (where the stress in the film is the lowest). Note that the wavelength is nearly constant along the length, only varying modestly due to the accordion effect (applied to each wave).

As indicated earlier, the amplitudes and wavelengths of the wrinkled surface are dependent upon the stress gradient. The finite element results of Figs. 12 and 13 show the evolution and the distribution in amplitude with macroscopic strain for the tapered geometries of Fig. 9, showing the gradient in wavelength and amplitude for K of 0.91 and 0.82. These results of Figs. 12 and 13 show that wrinkling progressively encompasses more of the film length as the macroscopic strain increases. They also show that the gradient in wrinkle amplitude over the length decreases with an increase in macroscopic strain: for $K = 0.91$, the gradient decreases by a factor of 5 as the strain increases from 2.9% to 4%; for $K = 0.82$, the gradient decreases by a factor of 3 as the strain increases from 2.9% to 4%.

6.3 Wrinkle Profiles: Experiments. Graded wrinkling was experimentally examined for the case of K of 0.91, 0.82, and 0.72 for the films described earlier where $\varepsilon_{macro} = 20\%$. Results are presented in Fig. 14 and Table 1. Figure 14 shows the wrinkle profile measures for the case of $K = 0.72$ in regions 1–3. In region 1 (lowest local strain and stress), $\lambda \approx 27.2\ \mu$m and $A \approx 3.12\ \mu$m; region 2, $\lambda \approx 24.4\ \mu$m and $A \approx 3.35\ \mu$m; region 3 (highest local strain and stress), $\lambda \approx 23.1\ \mu$m and $A \approx 3.86\ \mu$m—showing the gradient in wavelength and amplitude, noting that the ratios of the local strain prior to wrinkling in the regions are as ε_1: ε_2: $\varepsilon_3 \approx 0.7{:}0.85{:}1$. Table 1 reveals the wavelength and amplitude gradient to increase with a decrease in K. The case of $K = 0.91$ does not exhibit a gradient noting this is close to $K = 1$ which is the uniform case. Additionally, the finite element results in Sec. 6.2 showed that increase in the macroscopic strain results in reduction in the amplitude gradient along the length, and therefore with $\varepsilon_{macro} = 20\%$ the ratio of the amplitudes of the waves in regions 1 and 2 to the largest amplitude (region 3) in all the cases is larger than the values presented in Figs. 12 and 13.

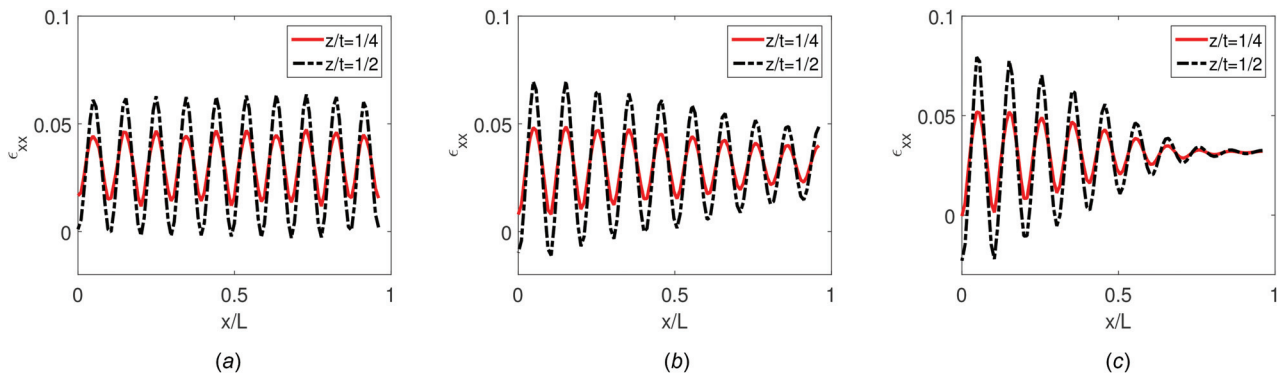

Fig. 11 Strain distribution in wrinkled films. The profiles are at $\varepsilon_{macro} = 4\%$ and $E_f/E_s = 100$. (*a*) Uniform wrinkling—$K = 1$, (*b*) graded wrinkling—$K = 0.91$, and (*c*) graded wrinkling—$K = 0.82$.

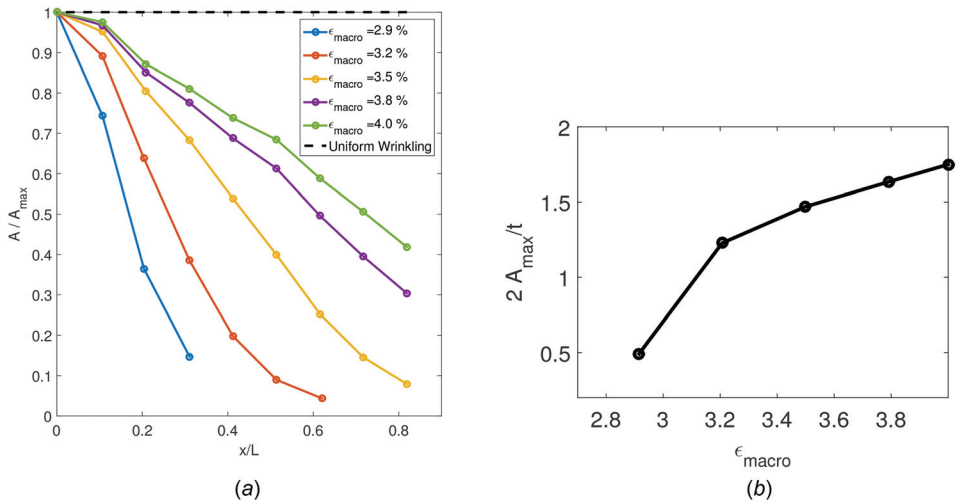

Fig. 12 Amplitudes of the waves in graded wrinkling for a trapezoidal geometry with $K = 0.91$: (*a*) trend in the amplitudes in graded wrinkling over different ε_{macro} for a trapezoidal geometry with $K = 0.91$ and (*b*) A_{max} of graded wrinkling at different ε_{macro}—A_{max} is the maximum amplitude at each macroscopic strain for a trapezoidal geometry with $K = 0.91$

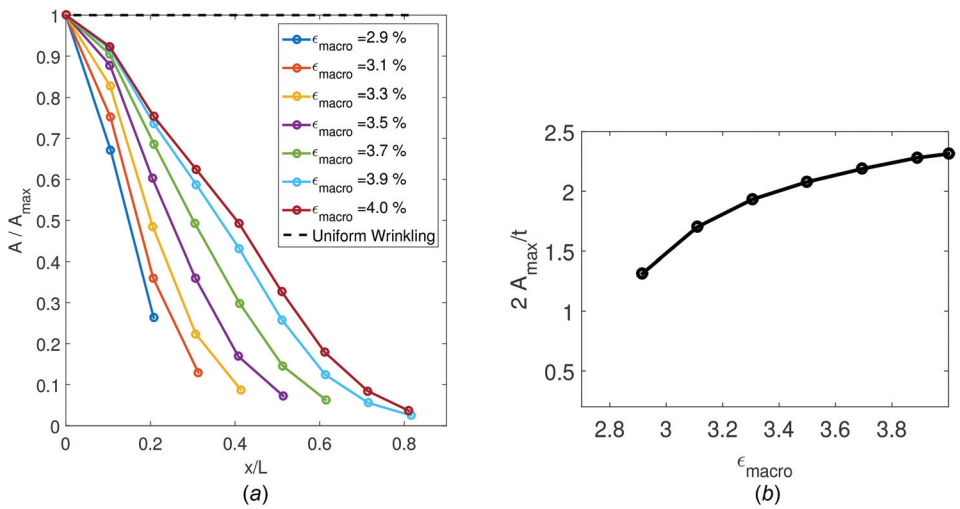

Fig. 13 Amplitudes of the waves in graded wrinkling for a trapezoidal geometry with $K = 0.82$: (*a*) trend in the amplitudes in graded wrinkling over different ε_{macro} for a trapezoidal geometry with $K = 0.82$ and (*b*) A_{max} of graded wrinkling at different ε_{macro}—A_{max} is the maximum amplitude at each macroscopic strain for a trapezoidal geometry with $K = 0.82$

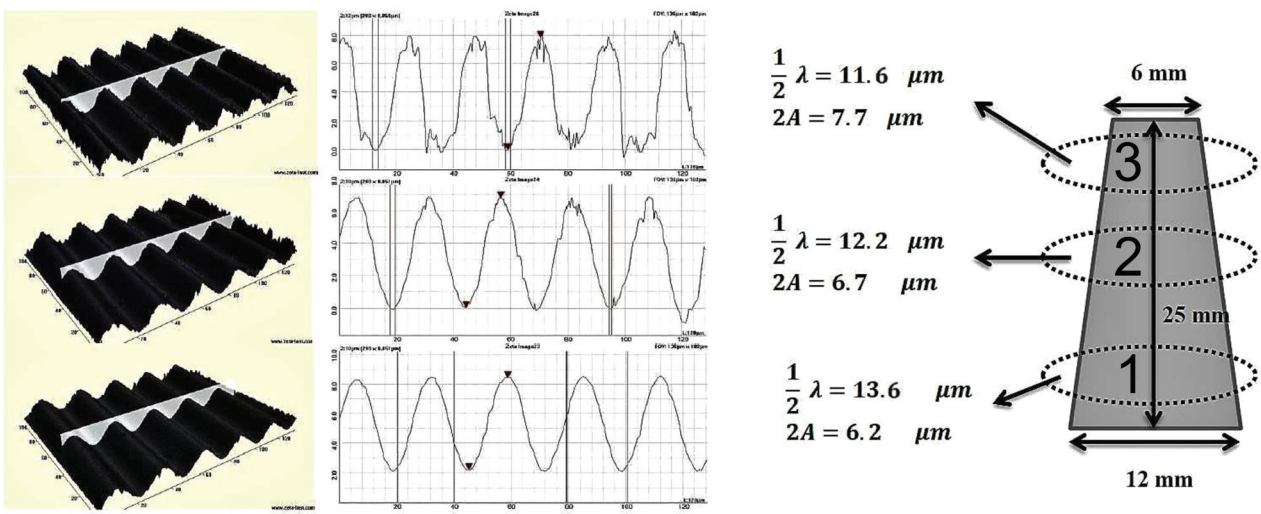

Fig. 14 Images of the experimental results of graded wrinkling on the sample geometry with $K = 0.72$ and $\varepsilon_{macro} = 20\%$

Table 1 Amplitude and wavelength of the wrinkles in the graded geometry with different values of K and $\varepsilon_{macro} = 20\%$. Regions 1–3 correspond to the regions shown in Fig. 5.

	Region 1		Region 2		Region 3	
K	A (μm)	λ (μm)	A (μm)	λ (μm)	A (μm)	λ (μm)
0.91	2.9	21.0	2.9	21.5	3.0	21.5
0.82	2.7	24.2	3.2	23.9	3.4	23.6
0.72	3.1	27.1	3.3	24.4	3.8	23.1

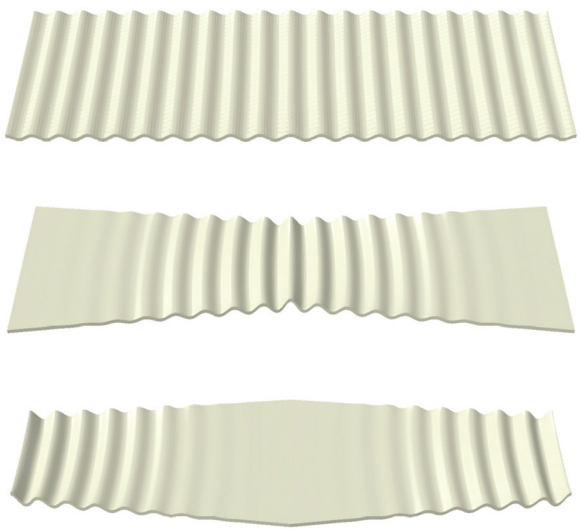

Fig. 15 Various configurations of graded wrinkling

It should also be noted that the analytical calculations only capture the critical point at which wrinkling is initiated, and as mentioned earlier finite element results are for small strains (up to 4% to avoid any nonlinear effects. Thus, only the trends in the amplitude and wavelength are compared with the theory and finite element results.

7 Conclusion

The ability to form surfaces with well-structured graded wrinkles via geometrically tailoring the uniaxial strain gradient in the film was shown through theory, numerical simulation, and experiment. Due to the geometric gradient in the film, the compressive strain and stress along the length of the film can be tailored to preferentially initiate wrinkling in different positions and provide an evolution in the cascading initiation of new wrinkles combined with the amplification of wrinkles that previously initiated. The geometric gradient provides a gradient in the initiation and the progression of the wrinkles. This gradient effect was quantitatively examined for linearly tapered geometries. For illustration, two examples of the same linear taper in geometry and the corresponding wrinkle profiles are shown in Fig. 15 together with the counterpart uniform case.

The initial wavelength and the critical strain under graded conditions are found to increase with an increase in gradient, but this critical wavelength is found to be the same along the length of the film. Hence, for well-structured gradients such as these linearly tapered geometries, the sequential initiation and progressive amplification of wrinkling along the length provide a highly structured evolution in wrinkling which can be used to tune surface properties both spatially and with macroscopic loading. More complex strain gradients can be designed to provide for more tailored graded wrinkle topologies.

Acknowledgment

This research was supported by the Center for Clean Water and Clean Energy at MIT and KFUPM.

Nomenclature

A = amplitude
A_0 = amplitude at the critical point
b = width of the film and substrate
b_L = largest width of the film at $x = L$
b_0 = smallest width of the film at $x = 0$
E_f = modulus of the film
E_s = modulus of the substrate
I_f = moment of inertia of the film
J_1 = Bessel function of the first kind
K = graded wrinkling geometric parameter
L = length of the film and substrate
P_f = compressive load applied to the film
t = film thickness
ν_f = Poisson ratio of the film
ν_s = Poisson ratio of the substrate
$w(x)$ = displacement of the film in the z direction
x, y, z = directions of the coordinate system
δ = macroscopic applied displacement in the x direction
ε = strain
ε_{cr} = critical strain
ε_{macro} = macroscopic strain
ε_{xx} = compressive normal strain in the x direction
η = ratio of the length of the film to the largest width of the film L/b_L
θ = taper angle in graded geometry
λ = wavelength
Λ = eigenvalue
λ_{cr} = critical wavelength
Λ_{cr} = critical eigenvalue
σ_f = compressive stress in the film
σ_{xx} = compressive normal stress in the x direction
σ_{xz} = xz component of shear stress
σ_{zz} = compressive normal stress in the z direction
Φ = modified stress function

Appendix: Solution of the Eigenvalue Problem

The governing equation of the thin film on the large elastic substrate using the beam theory which is the result of the equilibrium equation of the thin film and the distribution of the reaction of the substrate on the film are shown in the following equation (Fig. 16):

$$\frac{\partial^2}{\partial x^2}\left(E_f I_f \frac{\partial^2 w}{\partial x^2}\right) + P_f \frac{\partial^2 w}{\partial x^2} + \sigma_{zz} b(x) = 0\,;\ \ \sigma_{zz} b(x) = C\frac{\partial^2 w}{\partial x^2} \tag{A1}$$

Thus, substituting the substrate reactions into the governing equation results in the eigenvalue (Λ) problem (Eq. (A2))

$$\frac{\partial^2}{\partial x^2}\left(\frac{b(x)}{b_L}\frac{\partial^2 w}{\partial x^2}\right) + \Lambda^2 \frac{\partial^2 w}{\partial x^2} = 0\,;\ \ \Lambda^2 = \frac{P_f + C}{\frac{1}{12} E_f\, t\, b_L^3} \tag{A2}$$

In order to find C, the equilibrium equation for the substrate should be used. However, for such a nonuniform geometry, it is not possible to use the biharmonic equation and the stress function as defined in the uniform case [7,8]. In the uniform case, the substrate is assumed to have a response in the x–z plane, and the effect of the width of the substrate would cancel out since it is constant everywhere. However, in the graded wrinkling, the width is not constant, and thus the equilibrium equations will not be the same as the ones in uniform wrinkling. Using the free body

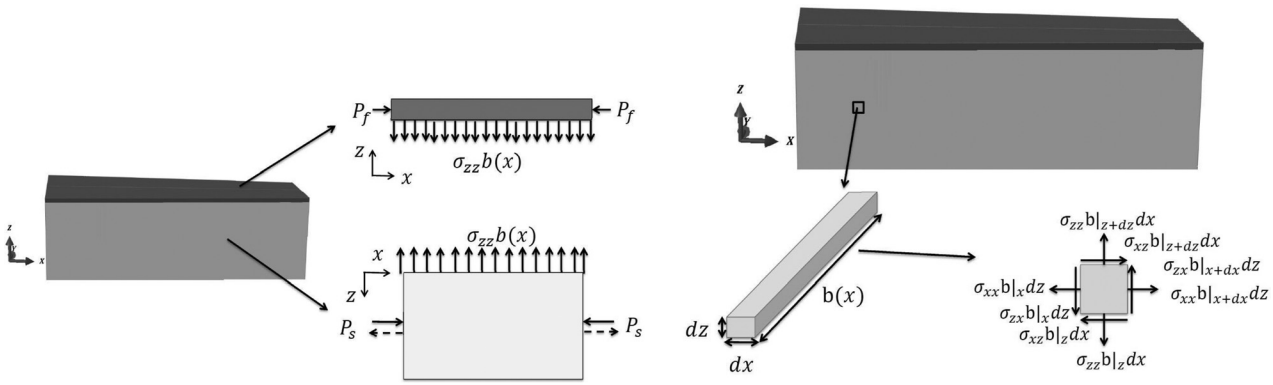

(*a*) (*b*)

Fig. 16 Free body diagram of the film and substrate under compressive loading: (*a*) free body diagram of the film and the substrate and (*b*) free body diagram of an infinitesimal element in the substrate

diagram of a strip element of the substrate, equilibrium equations can be found, and then combining their derivatives reduces the two equilibrium equations into the following equation:

$$\frac{\partial^2}{\partial x^2}(\sigma_{xx}b(x)) + \frac{\partial^2}{\partial x \partial z}(\sigma_{xz}b(x)) + \frac{\partial^2}{\partial z^2}(\sigma_{zz}b(x)) = 0 \tag{A3}$$

Due to $b(x)$ varying, a modified stress function can be defined as in the following equation:

$$\sigma_{xx}b(x) = \frac{\partial^2 \Phi}{\partial z^2}; \quad \sigma_{zz}b(x) = \frac{\partial^2 \Phi}{\partial x^2}; \quad \sigma_{xz}b(x) = -\frac{\partial^2 \Phi}{\partial x \partial z} \tag{A4}$$

Assuming that the stress in the transverse direction is negligible ($\sigma_{yy} = 0$), then the strains in the substrate can be defined as $\varepsilon_{xx} = 1/E_s(\sigma_{xx} - \nu_s\sigma_{zz})$, $\varepsilon_{zz} = 1/E_s(\sigma_{zz} - \nu_s\sigma_{xx})$, $\varepsilon xz = 1/G_s\sigma_{xz}$. Thus, combining Eq. (A3), Eq. (A4), and strain definitions with the compatibility equations, it can be shown that the modified stress function (Φ) satisfies the biharmonic equation ($\nabla^2\nabla^2\Phi = 0$). So, in order to find the stress state in the substrate, Φ should be found. Using the assumption in Eq. (A1) and combining with the definition in Eq. (A4), Φ can be related to the downward displacement of the film, known as $w(x)$ with $\partial^2\Phi/\partial x^2 = C\partial^2 w/\partial x^2$.

Knowing the value of σ_{zz} on top of the substrate, it is assumed that the expression for the stress can be expanded to the entire substrate by just multiplying by a function $g(x, z)$. This function should have a value of 1 on the top surface ($z = 0$) and decay away as z goes toward infinity. Therefore, σ_{zz} in the substrate can be defined as Eq. (A5) (similar to the uniform case), and thus the modified stress function can be found to be

$$\begin{aligned} \sigma_{zz}b(x) &= \left(C\frac{\partial^2 w}{\partial x^2}\right)(1+\alpha z)\exp(-\alpha z) \\ \rightarrow\ \Phi &= \int\int\left(C\frac{\partial^2 w}{\partial x^2}\right)(1+\alpha z)\exp(-\alpha z)\,dx\,dx \end{aligned} \tag{A5}$$

This form of a modified stress function satisfies the boundary condition of having no shear stress on the interface between the film and the substrate. In order to find C, the boundary condition of the substrate having the same displacement as the film at the interface ($z = 0$) is used. Knowing that the argument in the exponential should be dimensionless, with similar assumptions as the ones in uniform wrinkling, it can be assumed that $\alpha = \Lambda((2\tan(\theta)L)/(b_L\ln(b_L/b_0)))^{3/2}(b_L/b_0)^2$, and thus the modified stress function can be rewritten as

$$\begin{aligned} \Phi = \int\int\left(C\frac{\partial^2 w}{\partial x^2}\right)\left(1+\Lambda\left(\frac{2\tan(\theta)L}{b_L\ln\left(\frac{b_L}{b_0}\right)}\right)^{\frac{3}{2}}\left(\frac{b_L}{b_0}\right)^2 z\right) \\ \times\exp\left(-\Lambda\left(\frac{2\tan(\theta)L}{b_L\ln\left(\frac{b_L}{b_0}\right)}\right)^{\frac{3}{2}}\left(\frac{b_L}{b_0}\right)^2 z\right)dx\,dx \end{aligned} \tag{A6}$$

Therefore, using the displacement boundary condition at the interface of the film and the substrate gives

$$w = \frac{2A}{E_s b(x)\Lambda\left(\frac{2\tan(\theta)L}{b_L\ln\left(\frac{b_L}{b_0}\right)}\right)^{\frac{3}{2}}\left(\frac{b_L}{b_0}\right)^2}\frac{\partial^2 w}{\partial x^2} \tag{A7}$$

With the form of the eigenvalue equation presented in Eq. (A2) (Λ constant), it can be assumed that $\partial^2 w/\partial x^2 = -\Lambda^2 b_L/b(x)w$. Thus, by combining this equation with Eq. (A7), C can be found, and then substituting back into Eq. (A2) gives

$$\begin{aligned} C &= -\frac{E_s}{2\Lambda}\left(\frac{2\tan(\theta)L}{b_L\ln\left(\frac{b_L}{b_0}\right)}\right)^{\frac{3}{2}} b_L \\ \rightarrow\ P_f &= \frac{1}{12}E_f t b_L^3\Lambda^2 + \frac{E_s}{2\Lambda}\left(\frac{2\tan(\theta)L}{b_L\ln\left(\frac{b_L}{b_0}\right)}\right)^{\frac{3}{2}} b_L \end{aligned} \tag{A8}$$

Therefore, the critical load can be found by minimizing the load with respect to the eigenvalue, and thus the critical eigenvalue and the critical load in graded wrinkling are found to be

$$\begin{aligned} \Lambda_{\text{cr}} &= \frac{1}{t}\left(\frac{3E_s}{E_f}\right)^{\frac{1}{3}}\left(\frac{2\tan(\theta)L}{b_L\ln\left(\frac{b_L}{b_0}\right)}\right)^{\frac{1}{2}}; \\ \frac{P_{\text{cr}}}{E_f b_L t} &= \frac{1}{4}\left(\frac{3E_s}{E_f}\right)^{\frac{2}{3}}\left(\frac{2\tan(\theta)L}{b_L\ln\left(\frac{b_L}{b_0}\right)}\right)\frac{b_L}{b_0} \end{aligned} \tag{A9}$$

Now, in order to find the shape of the wrinkle profiles, Eq. (A1) should be solved. For solving the equation, intermediate variables are introduced

$$X = \frac{b(x)}{b_L} = \frac{b_L - 2(L-x)\tan\theta}{b_L} \rightarrow dX = \frac{2\tan\theta}{b_L}dx; \quad y = \frac{\partial^2 w}{\partial x^2} \tag{A10}$$

Substituting the two new variables into the general form gives

$$\frac{\partial^2}{\partial X^2}(Xy) + \frac{\Lambda_{cr}^2 {b_L}^2}{4\tan^2\theta}y = 0 \tag{A11}$$

Introducing two variables $u = \sqrt{X}$, $f = \sqrt{X}y$ and using the chain rule and manipulations give

$$u^2\frac{\partial^2 f}{\partial u^2} + u\frac{\partial f}{\partial u} + \left(\frac{\Lambda_{cr}^2 {b_L}^2}{\tan^2\theta}u^2 - 1\right)f = 0 \tag{A12}$$

Thus, solving Eq. (A12) using Bessel functions of the first kind results in

$$f = C_1 J_1\left(\frac{\Lambda_{cr} b_L}{\tan\theta}u\right) \rightarrow \frac{\partial^2 w}{\partial x^2} + C_2 = C_1\frac{J_1\left(\frac{\Lambda_{cr} b_L}{\tan\theta}\sqrt{X}\right)}{\sqrt{X}} + C_2 \tag{A13}$$

$$w(x) = \int\int C_1\frac{J_1\left(\frac{\Lambda_{cr} b_L}{\tan\theta}\sqrt{X}\right)}{\sqrt{X}}\,dx\,dx + C_2x^2 + C_3x + C_4 \tag{A14}$$

The integral can be solved to take the form of Eq. (A15) as

$$\begin{aligned} w(x) &= C_1\int\int\frac{J_1\left(\frac{\Lambda_{cr} b_L}{\tan\theta}\sqrt{\frac{b(x)}{b_L}}\right)}{\sqrt{\frac{b(x)}{b_L}}}\,dx\,dx + C_2x^2 + C_3x + C_4 \\ &= C_1\int\int\frac{J_1\left(\frac{\Lambda_{cr} L}{\tan\theta\,\eta}\sqrt{1-2\tan\theta\,\eta\frac{x}{L}}\right)}{\sqrt{1-2\tan\theta\,\eta\frac{x}{L}}}\,dx\,dx + C_2x^2 + C_3x + C_4 \\ &= \frac{-C_1}{\Lambda_{cr}^2}\sqrt{1-2\tan\theta\,\eta\frac{x}{L}}\,J_1\left(\frac{\Lambda_{cr} L}{\tan\theta\,\eta}\sqrt{1-2\tan\theta\,\eta\frac{x}{L}}\right) \\ &\quad + C_2x^2 + C_3x + C_4 \end{aligned} \tag{A15}$$

References

[1] Bechert, D., Bruse, M., and Hage, W., 2000, "Experiments With Three-Dimensional Riblets as an Idealized Model of Shark Skin," Exp. Fluids, **28**(5), pp. 403–412.

[2] Bhushan, B., 2011, "Biomimetics Inspired Surfaces for Drag Reduction and Oleophobicity/Philicity," Beilstein J. Nanotechnol., **2**, pp. 66–84.

[3] Bixler, G., and Bhushan, B., 2013, "Bioinspired Micro/Nanostructured Surfaces for Oil Drag Reduction in Closed Channel Flow," Soft Matter, **9**(5), pp. 1620–1635.

[4] Bixler, G. D., and Bhushan, B., 2013, "Fluid Drag Reduction and Efficient Self-Cleaning With Rice Leaf and Butterfly Wing Bioinspired Surfaces," Nanoscale, **5**(17), pp. 7685–7710.

[5] Feng, L., Li, S., Li, Y., Li, H., Zhang, L., Zhai, J., Song, Y., Liu, B., Jiang, L., and Zhu, D., 2002, "Super-Hydrophobic Surfaces: From Natural to Artificial," Adv. Mater., **14**(24), pp. 1857–1860.

[6] Zheng, Y., Gao, X., and Jiang, L., 2007, "Directional Adhesion of Superhydrophobic Butterfly Wings," Soft Matter, **3**(2), pp. 178–182.

[7] Allen, H. G., 1993, *Analysis and Design of Structural Sandwich Panels* (The Commonwealth and International Library: Structures and Solid Body Mechanics Division), Pergamon Press, Oxford, UK.

[8] Chen, X., and Hutchinson, J. W., 2004, "Herringbone Buckling Patterns of Compressed Thin Films on Compliant Substrates," ASME J. Appl. Mech., **71**(5), pp. 597–603.

[9] Cao, Y., and Hutchinson, J. W., 2012, "Wrinkling Phenomena in Neo-Hookean Film/Substrate Bilayers," ASME J. Appl. Mech., **79**(3), p. 031019.

[10] Yin, J., Yagüe, J. L., Eggenspieler, D., Gleason, K. K., and Boyce, M. C., 2012, "Deterministic Ordered Two-Dimensional Micro-Patterns of Thin Film on Soft Substrates Through Sequential Wrinkling," Adv. Mater., **24**(40), pp. 5441–5446.

[11] Jiang, H., Khang, D.-Y., Song, J., Sun, Y., Huang, Y., and Rogers, J. A., 2007, "Finite Deformation Mechanics in Buckled Thin Films on Compliant Supports," Proc. Natl. Acad. Sci. U. S. A., **104**(40), pp. 15607–15612.

[12] Volynskii, A., Bazhenov, S., Lebedeva, O., and Bakeev, N., 2000, "Mechanical Buckling Instability of Thin Coatings Deposited on Soft Polymer Substrates," J. Mater. Sci., **35**(3), pp. 547–554.

[13] Efimenko, K., Rackaitis, M., Manias, E., Vaziri, A., Mahadevan, L., and Genzer, J., 2005, "Nested Self-Similar Wrinkling Patterns in Skins," Nat. Mater., **4**(4), pp. 293–297.

[14] Moon, M., Lee, S., Sun, J., Oh, K., Vaziri, A., and Hutchinson, J., 2007, "Wrinkled Hard Skins on Polymers Created by Focused Ion Beam," Proc. Natl. Acad. Sci., **104**(4), pp. 1130–1133.

[15] Southern, E., and Thomas, A., 1965, "Effect of Constraints on the Equilibrium Swelling of Rubber Vulcanizates," J. Polym. Sci., Part A: Gen. Pap., **3**(2), pp. 641–646.

[16] Wang, L., Pai, C.-L., Boyce, M. C., and Rutledge, G. C., 2009, "Wrinkled Surface Topographies of Electrospun Polymer Fibers," Appl. Phys. Lett., **94**(15), p. 151916.

[17] Chan, E., Smith, E., Hayward, R., and Crosby, A., 2008, "Surface Wrinkles for Smart Adhesion," Adv. Mater., **20**(4), pp. 711–716.

[18] Bowden, N., Brittain, S., and Evans, A., 1998, "Spontaneous Formation of Ordered Structures in Thin Films of Metals Supported on an Elastomeric Polymer," Nature, **393**, pp. 146–149.

[19] Chen, X., and Yin, J., 2010, "Buckling Patterns of Thin Films on Curved Compliant Substrates With Applications to Morphogenesis and Three-Dimensional Micro-Fabrication," Soft Matter, **6**(22), pp. 5667–5680.

[20] Davis, C. S., and Crosby, A. J., 2012, "Wrinkle Morphologies With Two Distinct Wavelengths," J. Polym. Sci., Part B: Polym. Phys., **50**(17), pp. 1225–1232.

[21] Schweikart, A., and Fery, A., 2009, "Controlled Wrinkling as a Novel Method for the Fabrication of Patterned Surfaces," Microchim. Acta, **165**(3–4), pp. 249–263.

[22] Cerda, E., and Mahadevan, L., 2003, "Geometry and Physics of Wrinkling," Phys. Rev. Lett., **90**(7), p. 074302.